THE JOURNAL OF BIOLOGICAL CHEMISTRY VOL. 285, NO. 16, pp. 12299–12307, April 16, 2010

Crystal Structure of Human REV7 in Complex with a Human REV3 Fragment and Structural Implication of the Interaction between DNA Polymerase ζ and REV1*[S]

Received for publication, December 7, 2009, and in revised form, January 22, 2010 Published, JBC Papers in Press, February 17, 2010, DOI 10.1074/jbc.M109.092403

Kodai Hara (原幸大)[‡], **Hiroshi Hashimoto** (橋本博)[‡1], **Yoshiki Murakumo** (村雲芳樹)[§], **Shunsuke Kobayashi** (小林俊介)[¶], **Toshiaki Kogame** (小亀敏明)[¶], **Satoru Unzai** (雲財悟)[‡], **Satoko Akashi** (明石知子)[‡], **Shunichi Takeda** (武田俊一)[¶], **Toshiyuki Shimizu** (清水敏之)[‡], **and Mamoru Sato** (佐藤衛)[‡]

From the [‡]Graduate School of Nanobioscience, Yokohama City University, 1-7-29 Suehiro-cho, Tsurumi-ku, Yokohama 230-0045, Japan, the [§]Graduate School of Medicine, Nagoya University, 65 Tsurumai, Showa-ku, Nagoya 466-8550, Japan, and the [¶]Graduate School of Medicine, Kyoto University, Konoe Yoshida, Sakyo-ku, Kyoto 606-8501, Japan

DNA polymerase ζ (Polζ) is an error-prone DNA polymerase involved in translesion DNA synthesis. Polζ consists of two subunits: the catalytic REV3, which belongs to B family DNA polymerase, and the noncatalytic REV7. REV7 also interacts with REV1 polymerase, which is an error-prone Y family DNA polymerase and is also involved in translesion DNA synthesis. Cells deficient in one of the three REV proteins and those deficient in all three proteins show similar phenotype, indicating the functional collaboration of the three REV proteins. REV7 interacts with both REV3 and REV1 polymerases, but the structure of REV7 or REV3, as well as the structural and functional basis of the REV1-REV7 and REV3-REV7 interactions, remains unknown. Here we show the first crystal structure of human REV7 in complex with a fragment of human REV3 polymerase (residues 1847–1898) and reveal the mechanism underlying REV7-REV3 interaction. The structure indicates that the interaction between REV7 and REV3 creates a structural interface for REV1 binding. Furthermore, we show that the REV7-mediated interactions are responsible for DNA damage tolerance. Our results highlight the function of REV7 as an adapter protein to recruit Polζ to a lesion site. REV7 is alternatively called MAD2B or MAD2L2 and also involved in various cellular functions such as signal transduction and cell cycle regulation. Our results will provide a general structural basis for understanding the REV7 interaction.

Large numbers of DNA lesions occur daily in every cell, and the majority of the DNA lesions stall replicative DNA polymerases. This results in the arrest of DNA replication, which causes lethal effects including genome instability and cell death. Translesion DNA synthesis (TLS)[2] releases this replication blockage by replacing the stalled replicative polymerase with a DNA polymerase specialized for TLS (TLS polymerase). It is generally considered that TLS includes two steps performed by at least two types of TLS polymerases, namely inserter and extender polymerases (reviewed in Refs. 1 and 2). In the first step, the stalled replicative polymerase is switched to an inserter polymerase such as Polη, Polκ, Polι, or REV1, which are classified as Y family DNA polymerases (3) and have different lesion specificity (reviewed in Refs. 4–8), and an inserter polymerase incorporates nucleotides opposite the DNA lesion instead of the stalled replicative polymerase. In the second step, an inserter polymerase is switched to the extender polymerase DNA polymerase ζ (Polζ), and then Polζ extends a few additional nucleotides before a replicative polymerase restarts DNA replication.

Polζ consists of the catalytic REV3 and the noncatalytic REV7 subunits. REV3 is classified as a B family DNA polymerase on the basis of the primary sequence. The catalytic activity of yeast REV3 is stimulated by yeast REV7 (9). Biochemical analysis has been done only for yeast REV3 but not mammalian REV3, because the molecular mass of human REV3 is larger (~350 kDa) than that of yeast REV3 (~150 kDa). Disruption of the mouse *REV3* gene causes embryonic lethality accompanied by massive apoptosis (10–12), suggesting that the function of mammalian REV3 is essential for embryogenesis. Although REV7 is a smaller protein with a molecular mass of 24–28 kDa compared with REV3, the function of REV7 is less understood. REV7 is a member of the HORMA (Hop1, Rev7, and Mad2) family of proteins (13). REV7, which is alternatively called MAD2B or MAD2L2, appears to be involved in multiple cellular functions including not only TLS but also cell cycle regulation (14), bacterial infection (15), and signal transduction (16, 17).

In this study, we investigated the function of REV7 in TLS from structural analysis. Previous studies have reported that human REV7 interacts with the central region (residues 1847–1892) of human REV3 by yeast two-hybrid and *in vitro* interaction assays (18). Interestingly, human REV7 also interacts with the C-terminal region (residues 1130–1251) of human REV1 polymerase as

* This work was supported by funding from KAKENHI, the Protein 3000 Project, and the Target Protein Research Programs (to H. H., T. S., and M. S.), and by a grant from the Yokohama Academic Foundation (to H. H.).

[S] The on-line version of this article (available at http://www.jbc.org) contains supplemental Figs. S1 and S2.

The atomic coordinates and structure factors (codes 3ABD and 3ABE) have been deposited in the Protein Data Bank, Research Collaboratory for Structural Bioinformatics, Rutgers University, New Brunswick, NJ (http://www.rcsb.org/).

[1] To whom correspondence should be addressed. Tel.: 81-45-508-7227; Fax: 81-45-508-7365; E-mail: hash@tsurumi.yokohama-cu.ac.jp.

[2] The abbreviations used are: TLS, translesion DNA synthesis; Pol, polymerase; WT, wild type; GST, glutathione *S*-transferase; GFP, green fluorescent protein.

shown by yeast two-hybrid, *in vitro* interaction and co-immunoprecipitation assays (19–21). Furthermore, human REV7 and human REV1 were co-expressed by *Escherichia coli*, and the REV7-REV1 complex was purified, whereas REV7 does not affect the polymerase activity of REV1 (22). The three yeast *rev* mutants and the triple mutant show very similar sensitivity to various genotoxic treatments (23–25). Furthermore, chicken DT40 cells deficient in one of the three REV proteins and those deficient in all three proteins show hypersensitivity to various genotoxic treatment including cisplatin (*cis*-diaminedichloroplatinum (II)), indicating the functional collaboration of the three REV proteins (26). However, these previous analyses failed to determine the mechanism underlying the protein-protein interactions on the atomic revel, because they tried to analyze without data of the three-dimensional structures. In addition, it remains unclear whether mammalian REV1, REV3, and REV7 can form the Polζ-REV1 ternary complex. It has been considered that switching of DNA polymerase occurred at least twice in TLS: the switching from a stalled replicative polymerase to an inserter polymerase and from an inserter polymerase to the extender polymerase. Recently, the structural implications of the first polymerase switching have been reported (27). However, the mechanism underlying the recruitment of the extender polymerase to the lesion site and the second polymerase switching as well as the physical and functional interactions of REV1, REV3, and REV7 remains unclear. Here we report the first crystal structure of human REV7 in complex with a fragment of human REV3 (residues 1847–1898). The structure reveals the mechanism underlying Polζ formation and shows that the REV7-REV3 interaction unexpectedly provides a structural interface for REV1 binding. Furthermore, we show that these REV7-mediated interactions with REV1 and REV3 are responsible for DNA damage tolerance. Lastly, we propose a model of the structural interplay of REV1, REV3, and REV7 in TLS. Our results will provide a general structural basis for understanding the REV7 interaction in various cellular functions.

EXPERIMENTAL PROCEDURES

Crystallographic Analysis of Human REV7 in Complex with REV3 Fragment—In the present crystallographic study, REV7 with an R124A mutation, REV7(R124A), was used instead of wild type REV7, REV7(WT) (28). It has been shown that a human REV3 fragment (residues 1847–1892) interacts with human REV7 (18). Thus, based on the result of secondary structure prediction, we constructed the REV3 fragment carrying residues 1847–1898, REV3(1847–1898), for this crystallographic study (28). The REV7(WT)-REV3(1847–1898) complex was polydisperse and did not crystallize, whereas REV7(R124A)–REV3(1847–1898) complex was a monodisperse (28). In addition, REV7(R124A) efficiently binds REV3(1847–1898). Preparation and crystallization of the human REV7(R124A)-REV3(1847–1898) complex have been described before (28). In brief, recombinant human REV7(R124A) with an N-terminal hexameric His tag in complex with human REV3(1847–1898) was expressed in *E. coli* BL21(DE3) harboring the REV7(R124A)-REV3(1847–1898) co-expression vector. The protein was purified by nickel-Sepharose resin (GE Healthcare), HiTrap Q HP (GE Healthcare), and HiLoad Superdex200 (GE Healthcare). Monoclinic and tetragonal crystals of the REV7(R124A)-REV3(1847–1898) complex were obtained in different conditions. Heavy atom derivatives of monoclinic crystals were prepared by the soaking method using a solution of 10 mM ethylmercurithiosalicylate, 100 mM Tris-HCl, pH 7.5, 800 mM sodium formate, and 25% (w/v) polyethylene glycol 2000 monomethyl ether for 20 h. X-ray diffraction data for native crystals were collected by using a Quantum 315 CCD detector (Area Detector Systems Corp.) on Beamline BL-5A at Photon Factory. X-ray diffraction data for derivative crystals were collected by using an FR-D in-house x-ray generator with an R-AXIS IV^{++} imaging plate detector (Rigaku). All of the diffraction data were processed with the program HKL2000 (29). The structure of the REV7(R124A)-REV3(1847–1898) complex was solved by the single isomorphous replacement method using the programs SOLVE and RESOLVE (30, 31). Model building was performed with the programs O (32) and COOT (33). Structure refinement was performed at 1.9 Å resolution with the programs CNS (34) and REFMAC (35). $P2_1$ crystal contains two REV7(R124A)-REV3(1847–1898) complexes in the asymmetric unit. The structure in the $P4_12_12$ crystal was solved at 2.6 Å resolution by the molecular replacement method with the program MOLREP (36) using one of $P2_1$ structures. The structure was refined with a procedure similar to that of the monoclinic case. The data collection and refinement statistics are given in Table 1. The coordinates and structure factors have been deposited in the Protein Data Bank Japan.

In Vitro Interaction Assays—His-tagged REV7 protein was co-expressed with REV3(1847–1898) in *E. coli* BL21(DE3) as described before (28), and the cell lysate was applied to nickel-Sepharose resin (GE Healthcare). The beads were washed five times in a buffer (50 mM HEPES-NaOH, pH 7.4, 1.5 M NaCl, and 20 mM imidazole), and bound proteins were analyzed by SDS-PAGE with Coomassie Brilliant Blue stain. For interaction assays between the REV7-REV3(1847–1898) complex and REV1, GST fused the C-terminal region of human REV1(1130–1251), GST-REV1(1130–1251), was overexpressed in *E. coli* JM109 by isopropyl β-D-thiogalactopyranoside induction (1 mM at 25 °C), and was purified by glutathione-Sepharose 4B resin (GE Healthcare) by a standard procedure. In pull-down assays of the His-REV7-REV3(1847–1898) complex and GST-REV1(1130–1251), purified GST-REV1(1130–1251) was incubated with His-REV7-REV3(1847–1898) complex bound to the nickel-Sepharose resin (GE Healthcare) at 4 °C for 1 h. The beads were washed five times in a buffer (50 mM HEPES-NaOH, pH 7.4, 1.5 M NaCl, and 20 mM imidazole), and the bound proteins were analyzed by SDS-PAGE with Coomassie Brilliant Blue stain.

Co-immunoprecipitation Assays with HEK293 Cells—cDNA encoding wild type or mutant of human REV7 was inserted into a pEGFP-C2 vector (Clontech). cDNA encoding human REV1(826–1251) or REV3(1776–2044) (19) with an N-terminal FLAG sequence was inserted into a pcDNA3.1(+) vector (Invitrogen). For the co-immunoprecipitation assays, HEK293 cells were co-transfected with expression vectors for GFP-REV7 and FLAG-REV1(826–1251) or FLAG-REV3(1776–2044) using Lipofectamine 2000 (Invitrogen). The cells were disrupted in a buffer (20 mM HEPES-NaOH, pH 7.6, 300 mM NaCl, 0.1 mM EDTA, 10% glycerol, 1 mM dithiothreitol, 0.1%

Tween 20, 1 mM phenylmethylsulfonyl fluoride, and 10 mg/ml leupeptin) with freeze and thaw cycles. After adjusting the NaCl concentration to 150 mM, the cell lysates were clarified by centrifugation. The supernatants were incubated first with protein G-Sepharose beads (Sigma) and then with mouse monoclonal anti-FLAG M2 antibody (Sigma) for 2 h. The antigen-antibody complex was immobilized on protein G-Sepharose beads, and the beads were washed three times in a buffer (20 mM HEPES-NaOH, pH 7.6, 300 mM NaCl, 0.1 mM EDTA, 10% glycerol, 1 mM dithiothreitol, 0.1% Tween 20, 1 mM phenylmethylsulfonyl fluoride, and 10 mg/ml leupeptin). The bound proteins were analyzed by SDS-PAGE and Western blotting with anti-FLAG antibody or rabbit polyclonal anti-GFP antibody (MBL).

Rapid Survival Assays Using Chicken DT40 Cells—For retrovirus infection, a pMSCV-IRES-GFP recombinant plasmid was constructed by ligating the 5.2-kb BamHI-NotI fragment from pMSCVhyg (Clontech) with the 1.2-kb BamHI-Not1 fragment from pIRES2-EGFP (Clontech). cDNA of chicken REV7 (GdREV7) was inserted between the BglII and EcoRI sites of pMSCV-IRES-GFP. Virus was prepared by using 293T cells and 1 μl of Gene juice (Novagen), 1 μg of pMSCV-GdREV7-IRES-GFP, and 1 μg of pCL-Ampho. After the 293T cells were cultured with the above reagents and plasmids at 37 °C for 2 days, the cells were centrifuged, and the supernatant was stored at −80 °C. Retrovirus infection was done by centrifugation (3000 rpm, 30 min, 32 °C) of the DT40 *REV7*$^{-/-}$ cells (26) and the retroviral solution. A day after infection, expression of GFP was confirmed by flow cytometry. The efficiency of infection was more than 50%, as assayed by GFP expression. The cells were subcloned into 96-well plates, and clones displaying high levels of GFP were determined by a fluorescence-activated cell sorter. To test for differential sensitivity to cisplatin, we performed rapid survival assays using chicken DT40 cells.[3] The cells (1×10^4) were exposed to various concentrations of cisplatin and incubated at 39.5 °C for 48 h. We analyzed each cell type with at least three clones, and at least three independent experiments were carried out to obtain individual data. The cell number was counted by the Cell Titer-Glo luminescent cell viability assay (Promega) according to the manufacturer's instructions. We calculated the extent of cytotoxicity.

Figure Preparation—Fig. 1*B* was prepared with the programs Molscript (37) and Raster3D (38). Figs. 1*D*, 2*A*, and 3 (*A* and *C*) were prepared with the program PyMOL. Fig. 2*C* was prepared with the program TopDraw (39). All of the figures were modified by the programs PHOTOSHOP and ILLUSTRATOR (Adobe Systems).

RESULTS AND DISCUSSION

Overall Structure of Human REV7 in Complex with REV3 Fragment—We have determined the crystal structure of human REV7(R124A) in complex with human REV3(1847–1898) in two different crystal forms (Table 1). The structures in two different forms are essentially identical (supplemental Fig. S1), and thus we describe the higher resolution structure as a representative structure. REV7 is composed of three α-helices (αA, αB, and αC), eight β-strands (β2, β3, β4, β5, β6, β7′, β8′, and β8″), and three 3_{10} helices (3_{10}-1, 3_{10}-2, and 3_{10}-3) (Fig. 1, *A*–*C*). The REV3 fragment bound to REV7 comprises a β-strand (β^{REV3}) and an α-helix (α^{REV3}) (Fig. 1, *A*–*C*). Electron density of the N-terminal portion (residues 1847–1873 in the representative structure) of the REV3 fragment is not observed in all structures, indicating that the structure of the region is highly disordered. Three α-helices of REV7 are aligned on the same side of an anti-parallel β-sheet composed of β7′, β^{REV3}, β6, β4, β5, β8″, and β8′ and are flanked with an anti-parallel β-sheet comprising β2 and β3 on the other side. The C-terminal region following β6 (residues 153–211) of REV7 wraps around the REV3 fragment, resulting in a knot structure.

TABLE 1
Data collection and refinement statistics
The values in parentheses are those for the highest resolution shell (1.97–1.90, 2.90–2.80, and 2.69–2.60 Å for Native-1, Hg derivative, and Native-2, respectively).

	Native-1	Hg derivative	Native-2
Data collection			
Wavelength (Å)	1.0000	1.5418	1.0000
Space group	$P2_1$	$P2_1$	$P4_12_12$
a (Å)	43.8	43.8	76.5
b (Å)	50.0	49.9	76.5
c (Å)	107.2	107.5	118.5
α (°)	90	90	90
β (°)	96.9	96.9	90
γ (°)	90	90	90
Resolution (Å)	50.0-1.90	50.0-2.80	50.0-2.60
Observed reflections	129,606	43,119	61,068
Unique reflections	35,667	11,266	11,076
R-merge (%)	5.5 (26.8)	10.7 (29.7)	5.7 (31.4)
Completeness (%)	97.3 (83.1)	97.7 (96.6)	96.9 (81.8)
$\langle I \rangle / \sigma \langle I \rangle$	14.1 (3.7)	14.7 (7.0)	13.2 (3.1)
Refinement			
Resolution (Å)	20.0-1.90		20.0-2.60
Refined reflections	33,833		10,491
Free reflections	1,780		526
R-factor (%)	18.9		24.2
R-free (%)	24.1		28.1
Root mean square deviation bond lengths (Å)	0.020		0.018
Root mean square deviation bond angles (°)	1.689		1.782
Ramachandran plot			
Most favored (%)	91.6		84.6
Additional allowed (%)	8.4		12.8
Generously allowed (%)	0		2.6
Disallowed (%)	0		0
Protein Data Bank code	3ABD		3ABE

Human REV7 shares 22% amino acid identity with human Mad2, another member of the HORMA family (13). Mad2 functions in spindle assembly checkpoint by binding directly to Mad1 (40–42). Mad2 undergoes a striking conformational change from the open (O-Mad2) to the closed (C-Mad2) form, in which the C-terminal region known as the "seatbelt" following β6 moves toward the edge of β5 to wrap around the ligand, and β1 is relocated. Concomitantly, β7 and β8 are rearranged to form β8′ and β8″ (43, 44) (Fig. 1*A*). Structural alignment between REV7 bound to the REV3 fragment and Mad2 bound to Mad1 shows an root mean square deviation value of 2.0 Å for 183 superimposable Cα atoms (Fig. 1*D*), indicating that the overall structure of REV7 in the REV7(R124A)-REV3(1847–1898) complex may be very similar to the structure of the closed Mad2 form. Conceivably, a large conformational change may occur in the seatbelt (residues 153–211) of REV7 upon interaction with the REV3 fragment.

Structural Details of the Interaction between REV7 and REV3 in Polζ Formation—Our novel structural analysis of the human REV7(R124A)-REV3(1847–1898) complex allowed for the pre-

[3] T. Kogame and S. Takeda, unpublished data.

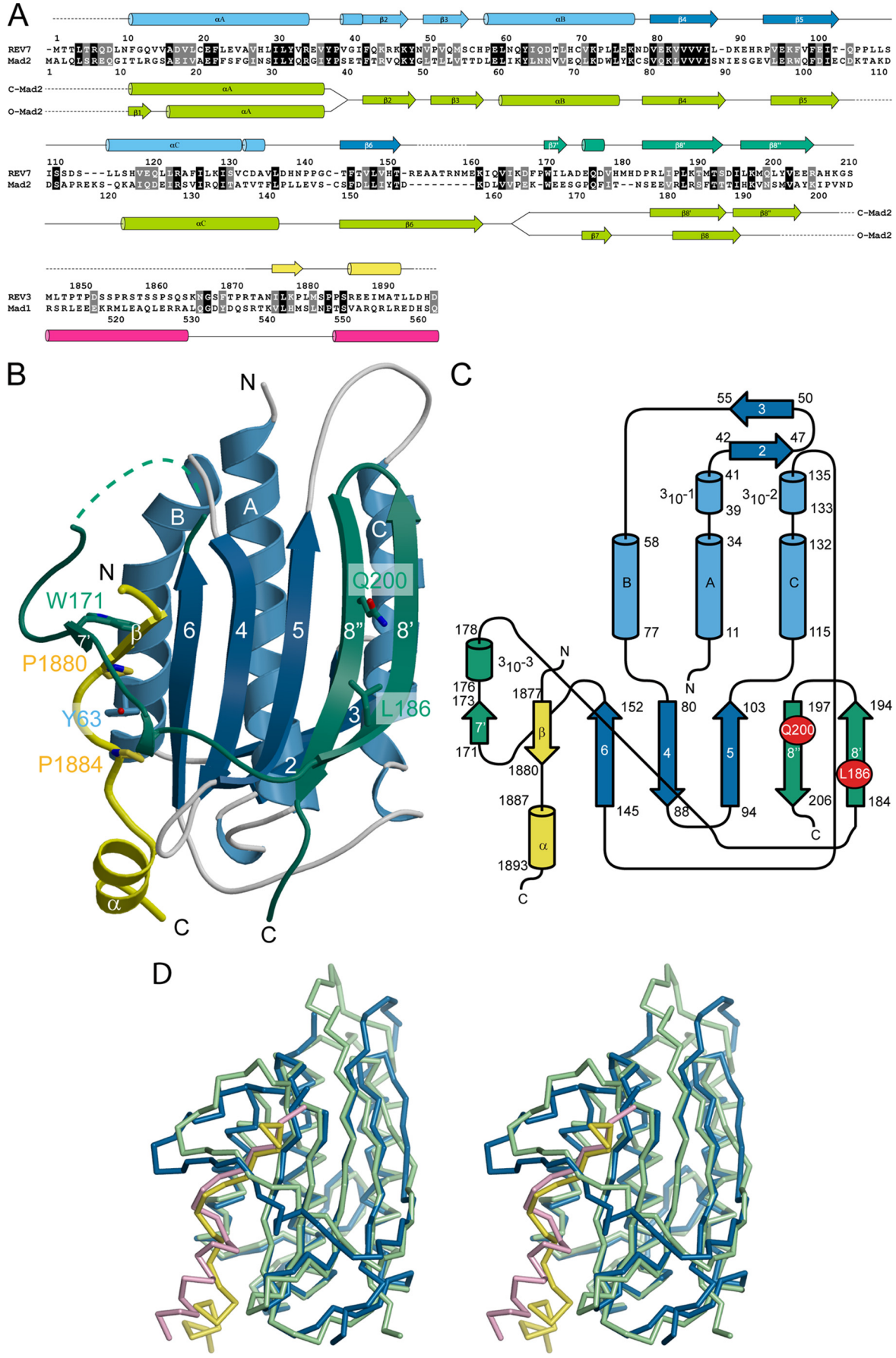
A
REV7
Mad2
C-Mad2
O-Mad2
REV3
Mad1
B
N
W171
P1880
Y63
P1884
Q200
L186
C
D

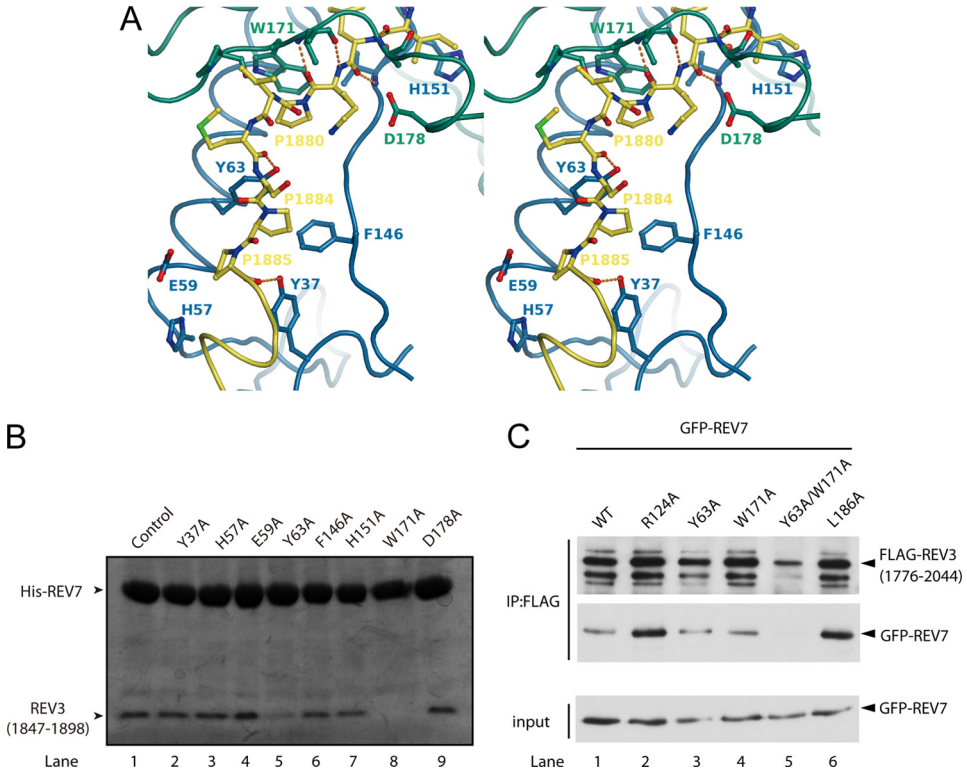

FIGURE 2. **Interactions between REV7 and REV3 fragment.** *A*, stereo view of structural details of the interactions between REV7 and REV3 fragment. REV7 is shown in *blue* and *green*, and REV3 is shown in *yellow*. Residues involved in the interaction are shown as stick models. *Orange dots* represent hydrogen bonds between REV7 and REV3. *B*, *in vitro* interactions between REV7 and REV3 fragment. His-REV7 mutant were co-expressed with REV3(1847–1898) in *E. coli*. Cell lysates were incubated on nickel-Sepharose beads. After washing, the bound proteins were resolved by SDS-PAGE with Coomassie Brilliant Blue stain. His-REV7(R124A) was used as a control binding to REV3(1847–1898) (*lane 1*). Y63A or W171A mutation significantly decreased the REV3 binding (*lane 5* or *8*). *C*, *in vivo* interactions between REV7 and REV3 fragment. GFP-REV7(WT) or GFP-REV7 mutant was co-expressed with FLAG-REV3(1776–2044) in HEK293 cells and incubated with Protein G beads. After washing, then proteins bound to beads were separated on SDS-PAGE and analyzed with Western blotting. Although GFP-REV7(Y63A) (*lane 3*) and GFP-REV7(W171A) (*lane 4*) retained binding affinity for FLAG-REV3(1776–2044), GFP-REV7(Y63A/W171A) showed no binding affinity for FLAG-REV3(1776–2044) (*lane 5*). GFP-REV7(R124A) showed higher binding affinity for FLAG-REV3(1776–2044), as compared with GFP-REV7(WT) (*lane 2*). REV7(L186A) lacking REV1 interaction (see Fig. 3, *C* and *D*) retained REV3 interaction (*lane 6*). *IP*, immunoprecipitation.

cise characterization of interactions between REV7 and REV3. β^{REV3} forms an anti-parallel β-sheet with $\beta6$ and $\beta7'$ of REV7. In addition to the hydrogen bonds in the β-sheet formation, the Oη atoms of two tyrosines, Tyr-37^{REV7} and Tyr-63^{REV7}, interact with the carbonyl oxygen atoms of Pro-1885^{REV3} and Met-1882^{REV3}, respectively. Furthermore, the aromatic rings of Tyr-63^{REV7} and Trp-171^{REV7} stack with the aliphatic rings of Pro-1884^{REV3} and Pro-1880^{REV3}, respectively (Fig. 2*A*). In addition, van der Waal's interactions between REV7 and the α-helix of REV3(1847–1898) are observed. The aromatic residues Tyr-37^{REV7}, Tyr-63^{REV7}, and Trp-171^{REV7} are highly conserved between yeast and human REV7, whereas Pro-1884^{REV3} and Pro-1880^{REV3} are conserved only in vertebrates, suggesting that the hydrophobic interactions are conserved at least in higher eukaryotes. To understand the role of individual amino acid residues of REV7 and REV3 in their physical interaction, we compared REV7-REV3 interactions with Mad2-Mad1 interactions. In the Mad2-Mad1 complex, Tyr-64^{Mad2} and Trp-167^{Mad2}, which correspond to Tyr-63^{REV7} and Trp-171^{REV7} (Fig. 1*A*), respectively, interact with Pro-549^{Mad1} and Met-545^{Mad1} in a hydrophobic manner, as observed in the REV7(R124A)-REV3(1847–1898) complex. In addition, Mad1 interacts significantly with the seatbelt region of Mad2, where the Nζ atom of Lys-541^{Mad1} forms hydrogen bonds with the main chain oxygen atoms of Lys-159^{Mad2} and Leu-161^{Mad2}. *In vitro* binding assays have revealed that not only Pro-549^{Mad1} but also Lys-541^{Mad1} is crucial for the Mad2-Mad1 interaction (44). However, a similar interaction observed in the Mad2-Mad1 complex is not observed in the REV7(R124A)-REV3(1847–1898) complex, implying that the mechanism underlying the REV7-REV3 interaction may be distinct from that of Mad2-Mad1 interaction. To elucidate the crucial residues responsible for the REV7-REV3 interaction, we performed *in vitro* binding assays using alanine mutants of REV7. Of these mutants, Y63A or W171A mutation significantly reduced affinity for REV3(1847–1898), indicating that Tyr-63^{REV7} and Trp-171^{REV7} are crucial for the physical interaction with REV3(1847–1898) (Fig. 2*B*, *lanes 5* and *8*). In contrast, Lys-159^{Mad2}, Leu-161^{Mad2}, Tyr-64^{Mad2}, and Trp-167^{Mad2} were crucial for the physical interaction with Mad1 in the Mad2-Mad1 interaction (44). Thus, the mechanism underlying

FIGURE 1. **Structure of human REV7 in complex with human REV3 fragment.** *A*, secondary structures and structure-based sequence alignment of human REV7 and Mad2 and human REV3 and Mad1. The secondary structure elements of human REV7 and REV3(1847–1898) are drawn above the sequences. The colors of the elements correspond to those of *B*. The partial sequence of human Mad1 (residues 512–563) corresponding to REV3(1847–1898) is shown. The secondary structure elements of human Mad2 and Mad1 are drawn below the sequences. The identical and homologous residues are shown on *black* and *gray* backgrounds, respectively. The nomenclature of the secondary structures of REV7 is based on those of Mad2. *B*, overall structure of human REV7 in complex with REV3 fragment. Structure of human REV7 in complex with REV3 fragment is shown by ribbon representations. The secondary structural elements are labeled. N- and C-terminal of REV7 and REV3 are also labeled. The loops not located in the electron density (residues 155–160) are shown as *dashed lines*. REV7 is colored *light blue* and *blue*. REV3 (1874–1895) is colored *yellow*. The C-terminal region of REV7 (residues 153–211) corresponding to the seatbelt of MAD2 is shown in *green*. Tyr-63 and Trp-171, which are responsible for interaction with REV3, are shown as stick models. Leu-186 and Gln-200, which are significantly involved in interaction with the C-terminal region of REV1, are also shown as stick models. *C*, topology diagram of the REV7-REV3 complex. The secondary structural elements are labeled. N- and C-terminal of REV7 and REV3 are also labeled. The colors of the structural elements correspond to those of *B*. Leu-186 and Gln-200 responsible for REV1 binding are shown by *red ellipsoids*. *D*, stereo view of superimposed structures of the REV7-REV3 and Mad2-Mad1 complexes. REV7, REV3, Mad2, and Mad1 are shown in *blue*, *yellow*, *green*, and *pink*, respectively. To simplify, a partial structure (residues 540–560) of Mad1 is shown.

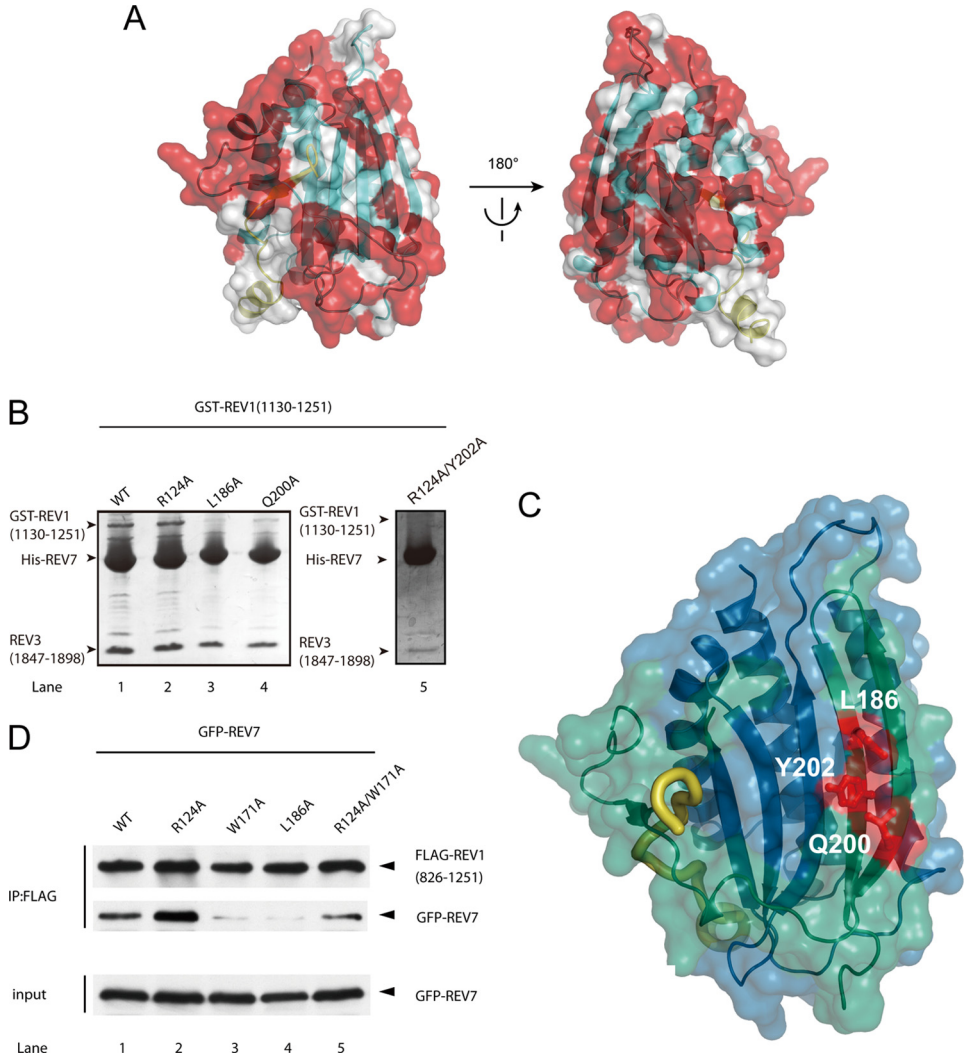

FIGURE 3. **Interactions with the C-terminal region of REV1.** *A*, molecular surface of REV7 in complex with REV3 fragment. The structure is shown by ribbon drawing and transparent molecular surface. Residues mutated in REV7 in this work are shown in *red* on the transparent surface. Two different views are shown to provide a clearer perspective of residues mutated in REV7. *B*, *in vitro* interactions between the REV7-REV3 complex and the C-terminal region of REV1. Purified GST-REV1(1130–1251) was incubated with a His-REV7-REV3(1847–1898) complex bound to nickel-Sepharose beads. After washing, the bound proteins were resolved by SDS-PAGE. His-REV7(L186A) (*lane 3*), His-REV7(Q200A) (*lane 4*), and His-REV7(Y202A) (*lane 5*) decreased REV1 binding. *C*, the REV1-binding site on the molecular surface of the REV7-REV3 complex. REV7 is shown as a ribbon drawing and transparent molecular surface. REV3 fragment is shown as a *yellow tube*. Leu-186, Gln-200, and Tyr-202 responsible for REV1 binding are indicated in *red*, and these residues form the platform for REV1 binding. *D*, *in vivo* interactions between REV7 and the C-terminal region of REV1. GFP-REV7(WT) or GFP-REV7 mutant was co-expressed with FLAG-REV1(826–1251) in HEK293 cells and incubated with protein G beads. After washing, the proteins bound to beads were separated on SDS-PAGE and analyzed with Western blotting. GFP-REV7(L186A) (*lane 4*) showed no binding affinity for FLAG-REV1(826–1251), although this mutant showed binding affinity for FLAG-REV3(1776–2044) (see Fig. 2*C*). GFP-REV7(W171A) (*lane 3*) showed no binding affinity for FLAG-REV1(826–1251), whereas the GFP-REV7(R124A/W171A) mutant showed binding affinity for FLAG-REV1(826–1251). *IP*, immunoprecipitation.

the REV7-REV3 interaction is distinctly different from that underlying the Mad2-Mad1 interaction. In addition, the α-helix of REV3(1847–1898) might be required for interaction with REV7, because a REV3 fragment (residues 1847–1886) lacking the α-helix did not form a stable complex with REV7 (data not shown). This suggests that the van der Waal's interactions by the α-helix of REV3(1847–1898) also contribute to the formation of the REV7-REV3 complex, Polζ.

Furthermore, to investigate the REV7-REV3 interaction *in vivo*, we carried out co-immunoprecipitation assays using HEK293 cells. Consistent with the *in vitro* results, REV7(Y63A/W171A) showed no binding affinity for REV3(1776–2044), although REV7(Y63A) and REV7(W171A) retained affinity (Fig. 2*C*, *lanes 3–5*). It is also noteworthy that the expression level of FLAG-REV3(1776–2044) in *lane 5* of Fig. 2*C* is considerably lower compared with other lanes, even though the same amount of plasmid DNA was used for transfection in each cells, suggesting that REV7-unbound REV3(1776–2044) may be unstable *in vivo*. Interestingly, REV7(R124A) had markedly higher affinity for REV3(1776–2044), as compared with REV7(WT) (Fig. 2*C*, *lane 2*). This observation suggests that the R124A substitution stabilized the closed conformation of REV7. In fact, the analogous substitution in Mad2, Mad2(R133A), pushes the conformation toward the closed form and enables structure determination of the ligand-free C-Mad2 (45), although why this substitution stabilizes the closed form is less understood. The CD spectrum of the REV7(R124A)-REV3(1847–1898) complex is similar to that of the REV7(WT)-REV3(1847–1898) complex (28), whereas the CD spectrum of REV7(R124A) is distinct from that of REV7(WT) (supplemental Fig. S2). This observation indicates that REV7 also supposedly undergoes a significant structural change, in which the seatbelt region is expected to move upon the ligand binding as observed in Mad2.

Structural Implication of the Interactions between Polζ and REV1—REV7 interacts with not only the central region (residues 1847–1892) of REV3 but also the C-terminal region (residues 1130–1251) of REV1 (reviewed in Ref. 46). The amino acid sequences of the REV7-interacting regions of REV3 and REV1 are not conserved, indicating that REV7 independently binds REV3 and REV1. However, it has remained unknown whether the human REV7-REV3 complex interacts with REV1. To investigate the physical interactions of the REV7-REV3(1847–1898) complex with REV1(1130–1251), we performed *in vitro* binding assay. Our results show that both the REV7(WT)-REV3(1847–1898) and REV7(R124A)-REV3(1847–1898) complexes interact with REV1(1130–1251) (Fig. 3*B*, *lanes 1* and *2*), indicating that REV7

simultaneously interacts with REV1(1130–1251) and REV3(1847–1898) using different interfaces of REV7.

To identify amino acid residues of REV7 responsible for interaction with REV1, we performed comprehensive alanine substitutions in the solvent-exposed residues of REV7 (Fig. 3*A*). Mad2 has two independent binding sites for different proteins; one is the seatbelt region, where Mad1 interacts with Mad2, and the other is the αC helix, which is the binding site of O-Mad2 for checkpoint activation (47) or $p31^{comet}$ for checkpoint inhibition (48). However, mutations in the αC helix in REV7 did not affect binding to REV1(1130–1251) (data not shown). Our results show that L186A or Q200A mutation significantly depletes REV1 binding, whereas those mutations have no effect on REV3 binding (Fig. 3*B*, *lanes 3* and *4*). The fact that Leu-186 and Gln-200 are exposed to solvent (Fig. 3*C*) indicates that these residues are directly involved in REV1 binding. Leu-186 and Gln-200 are present in β8′ and β8″, respectively (Fig. 3*C*). Therefore, the REV1-binding site is unprecedented and represents a novel interface for protein-protein interactions of HORMA family proteins. Consistent with this finding, Leu-186 and Gln-200 are not conserved in Mad2 (Fig. 1*A*), whereas they are conserved in yeast REV7. Leu-186 and Gln-200 of REV7 are positioned close to each other and are thus likely to provide a platform for REV1 binding on the anti-parallel β-sheet composed of β8′ and β8″. This observation implies that formation of the C-terminal β-sheet is significant for REV1 binding. To verify this idea, we performed further surveys by alanine substitution for residues that are relatively buried and seemingly involved in stabilizing the structure of the β-sheet. Consequently, we found that the Y202A mutation impaired the REV1 interaction (Fig. 3*B*, *lane 5*). Tyr-202 is located in β8″ and directly interacts with both Leu-186 and Gln-200 (Fig. 3*C*). These results indicate that Tyr-202 stabilizes the REV1-binding platform.

To examine whether $Leu\text{-}186^{REV7}$ is important for interaction with REV1 *in vivo*, we performed binding assays using human cells and showed that the L186A mutation greatly reduced the interaction with REV1(826–1251), although it did not reduce the interaction with REV3(1776–2044) (Fig. 2*C*, *lane 6*, and 3*D*, *lane 4*). On the other hand, the W171A mutation unexpectedly decreased the interaction with not only REV3(1776–2044) but also REV1(826–1251) (Fig. 3*D*, *lane 3*). Most interestingly, the R124A mutation, which stabilized the closed conformation of REV7, increased REV1 binding; furthermore, the double mutation R124A/W171A in REV7 brought back REV1 binding to the level of REV7(WT) (Fig. 3*D*, *lanes 2*, *3*, and *5*). Therefore, we conclude that REV1 interacts with the closed form of REV7 and that the REV7-REV3 interaction precedes the REV7-REV1 interaction during formation of the Polζ-REV1 complex.

Functional Role of REV7-mediated Interactions in DNA Damage Tolerance—To examine the contribution of REV7-mediated interactions to DNA damage tolerance, we performed rapid survival assays using chicken DT40 cells. Chicken REV7 shares a high degree of amino acid identity with human REV7 (96%). To functionally analyze the REV7-mediated interactions, we expressed chicken REV7(WT) and REV7(Y63A/W171A) in DT40 $REV7^{-/-}$ cells and measured the sensitivity

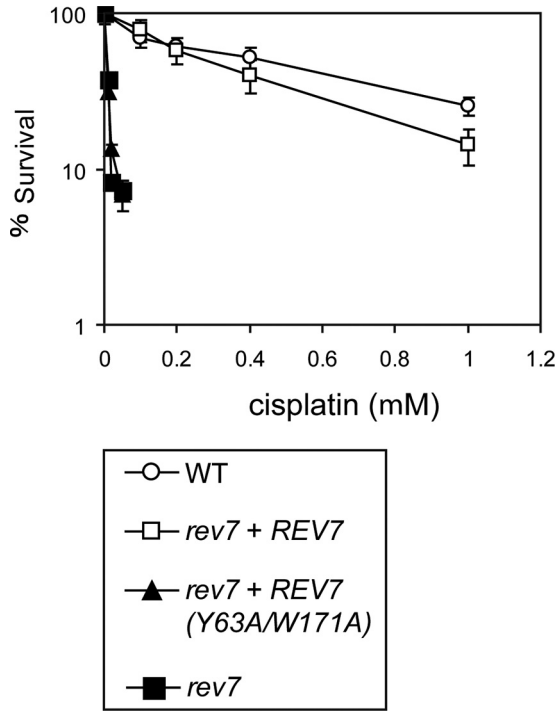

FIGURE 4. **Sensitivities of REV7 mutant cells to cisplatin using chicken DT40 cells.** The results of the rapid survival assays after treatment with cisplatin are indicated. The *symbols* indicating each genotype, shown at the *bottom*, represent the mean values of at least three clones and at least three independent experiments. Each *error bar* shows the standard deviation of the mean. The dose of cisplatin is displayed on the *horizontal axis* on a linear scale, and the percentile fractions of surviving cells are displayed on the *vertical axis* on a logarithmic scale.

to cisplatin in the resulting reconstituted clones (Fig. 4). We chose cisplatin, because $REV1^{-/-}$, $REV3^{-/-}$, or $REV7^{-/-}$ DT40 cells show strong sensitivity to cisplatin (26, 49). The reconstitution of $REV7^{-/-}$ cells with the REV7 transgene completely normalized cellular sensitivity to cisplatin (*white square*). In contrast, expression of REV7(Y63A/W171A), which lack both REV3 and REV1 interactions, had no impact on cellular sensitivity of $REV7^{-/-}$ cells to cisplatin (*black triangle*). Our results clearly indicate that REV7-mediated interactions are essential for resistance to the DNA damage caused by cisplatin, implying that formation of the Polζ-REV1 complex is responsible for resistance and that REV7 functions as an adapter protein between REV3 and REV1 polymerases.

Recruitment of Polζ and Polymerase Switching—Taking our results altogether, we can propose a model of the interactions involving REV1, REV3, and REV7 (Fig. 5*A*). In the absence of REV3, REV7 can adopt an open form. In the presence of REV3, REV7 undergoes structural rearrangement of the seatbelt by REV3 binding, resulting in the formation of Polζ, where $Tyr\text{-}63^{REV7}$ and $Trp\text{-}171^{REV7}$ are crucial for the interaction (Fig. 2). The conformational change in the seatbelt of REV7 provides an interface for REV1 interaction (Fig. 3*C*) and therefore enables formation of the Polζ-REV1 complex. REV1, which is the inserter polymerase for an abasic lesion (50, 51), is also supposed to function as a scaffold protein for polymerase switching at a lesion site, because the C-terminal region (residues 1130–1251) of REV1 interacts with the other inserter polymerases, namely Polη, Polκ, and Polι (21). In addition, it has been shown

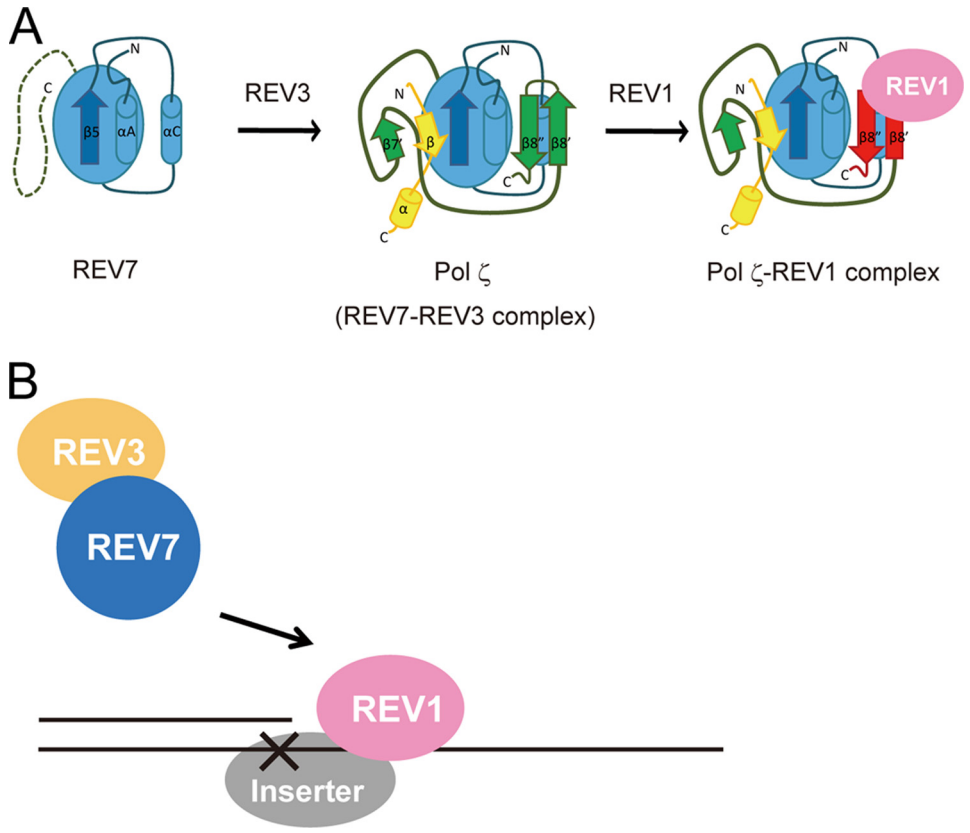

FIGURE 5. **Model of the interaction of REV1, REV3, and REV7.** *A*, formation of the Polζ-REV1 complex. Schematic drawings of opened REV7, REV7-REV3, and Polζ-REV1 complexes are shown in the *left*, *middle* and *right panels*, respectively. The *colors* of REV7 and REV3 correspond to those in Fig. 1*B*. In the Polζ-REV1 complex, the *β8′* and *β8″* strands of REV7 are shown by *red*. REV1 is shown by a *pink ellipsoid*. *B*, recruitment of Polζ to a lesion site via REV7-REV1 interaction. REV7, REV3, and REV1 are shown by *blue*, *yellow*, and *pink ellipsoids*, respectively. An inserter polymerase located in a lesion site is also shown by *gray ellipsoid*. ×indicates a lesion site in the template DNA strand.

that mouse Polκ and Rev7 compete directly for binding to Rev1 (20). Based on our results, we can propose a model of the recruitment of Polζ and the second polymerase switching from an inserter polymerase to the extender polymerase, as well (Fig. 5*B*). An inserter polymerase suitable for a DNA lesion could perform bypass synthesis after the first polymerase switching from a replicative polymerase to an inserter polymerase through interactions with ubiquitinated PCNA and/or the C-terminal region of REV1. Then Polζ (REV7-REV3 complex) could be recruited to the lesion site by the interaction between REV7 and the C-terminal region of REV1, where the C-terminal β-sheet of REV7 is crucial. The REV7-REV1 interaction would release an inserter polymerase from the C-terminal region of REV1, and Polζ subsequently could perform extension from the nucleotide inserted by an inserter polymerase (Fig. 5*B*). Depending on DNA lesions, it is considered that Polζ performs both nucleotide insertion and extension. In this case, Polζ is recruited to the lesion site through the REV7-REV1 interaction in a similar way. In contrast to the interaction of human REV7 and REV1, it has been reported that yeast Rev7 interacts with various regions of yeast Rev1 (the N-terminal BRCT domain; the polymerase-associated domain, which is alternatively called the little finger domain; and the C-terminal domain) (52–54). Furthermore, yeast Polη, an inserter polymerase, interacts with the polymerase-associated domain of yeast Rev1 (55). Therefore, the Rev1 interactions in yeast are complicated, and the interactions might diverge between yeast and human.

In this work, we have performed structural and functional analysis of REV7-mediated interactions, and clarified the structural basis of the REV7-REV3 interaction and obtained structural implication of Polζ-REV1 interactions. We propose that REV7 functions as the adapter protein between REV3 and REV1 polymerases, thereby mediating the second polymerase switching. Human REV7 interacts with various proteins including the *Shigella* effector IpaB in bacterial infection and ELK1 and TCF4 in signal transduction (15–17). Those proteins have sequences similar to the REV7-binding region of human REV3, indicating that the mechanisms underlying the interactions of those proteins with REV7 are similar to that of the REV7-REV3 interactions described here. Thus, our finding will provide a general structural basis for understanding the interactions mediated by REV7 in various cellular functions.

Acknowledgment—We thank the beamline staff at Photon Factory, KEK, Japan, for data collection.

REFERENCES

1. Moldovan, G. L., Pfander, B., and Jentsch, S. (2007) *Cell* **129,** 665–679
2. Friedberg, E. C., Lehmann, A. R., and Fuchs, R. P. (2005) *Mol. Cell* **18,** 499–505
3. Ohmori, H., Friedberg, E. C., Fuchs, R. P., Goodman, M. F., Hanaoka, F., Hinkle, D., Kunkel, T. A., Lawrence, C. W., Livneh, Z., Nohmi, T., Prakash, L., Prakash, S., Todo, T., Walker, G. C., Wang, Z., and Woodgate, R. (2001) *Mol. Cell* **8,** 7–8
4. Vaisman, A., Lehmann, A. R., Woodgate, R., and Wei, Y. (2004) *Adv. Protein Chem.* **69,** 205–228
5. Ohmori, H., Ohashi, E., and Ogi, T. (2004) *Adv. Protein Chem.* **69,** 265–278
6. Lawrence, C. W. (2004) *Adv. Protein Chem.* **69,** 167–203
7. Prakash, S., Johnson, R. E., and Prakash, L. (2005) *Annu. Rev. Biochem.* **74,** 317–353
8. Guo, C., Kosarek-Stancel, J. N., Tang, T. S., and Friedberg, E. C. (2009) *Cell Mol. Life Sci.* **66,** 2363–2381
9. Nelson, J. R., Lawrence, C. W., and Hinkle, D. C. (1996) *Science* **272,** 1646–1649
10. Bemark, M., Khamlichi, A. A., Davies, S. L., and Neuberger, M. S. (2000) *Curr. Biol.* **10,** 1213–1216
11. Wittschieben, J., Shivji, M. K., Lalani, E., Jacobs, M. A., Marini, F., Gearhart, P. J., Rosewell, I., Stamp, G., and Wood, R. D. (2000) *Curr. Biol.* **10,**

1217–1220
12. Esposito, G., Godindagger, I., Klein, U., Yaspo, M. L., Cumano, A., and Rajewsky, K. (2000) *Curr. Biol.* **10,** 1221–1224
13. Aravind, L., and Koonin, E. V. (1998) *Trends Biochem. Sci.* **23,** 284–286
14. Chen, J., and Fang, G. (2001) *Genes Dev.* **15,** 1765–1770
15. Iwai, H., Kim, M., Yoshikawa, Y., Ashida, H., Ogawa, M., Fujita, Y., Muller, D., Kirikae, T., Jackson, P. K., Kotani, S., and Sasakawa, C. (2007) *Cell* **130,** 611–623
16. Zhang, L., Yang, S. H., and Sharrocks, A. D. (2007) *Mol. Cell. Biol.* **27,** 2861–2869
17. Hong, C. F., Chou, Y. T., Lin, Y. S., and Wu, C. W. (2009) *J. Biol. Chem.* **284,** 19613–19622
18. Murakumo, Y., Roth, T., Ishii, H., Rasio, D., Numata, S., Croce, C. M., and Fishel, R. (2000) *J. Biol. Chem.* **275,** 4391–4397
19. Murakumo, Y., Ogura, Y., Ishii, H., Numata, S., Ichihara, M., Croce, C. M., Fishel, R., and Takahashi, M. (2001) *J. Biol. Chem.* **276,** 35644–35651
20. Guo, C., Fischhaber, P. L., Luk-Paszyc, M. J., Masuda, Y., Zhou, J., Kamiya, K., Kisker, C., and Friedberg, E. C. (2003) *EMBO J.* **22,** 6621–6630
21. Ohashi, E., Murakumo, Y., Kanjo, N., Akagi, J., Masutani, C., Hanaoka, F., and Ohmori, H. (2004) *Genes Cells* **9,** 523–531
22. Masuda, Y., Ohmae, M., Masuda, K., and Kamiya, K. (2003) *J. Biol. Chem.* **278,** 12356–12360
23. Lawrence, C. W., and Christensen, R. B. (1979) *Genetics* **92,** 397–408
24. Lawrence, C. W., and Christensen, R. B. (1982) *Mol. Gen. Genet.* **186,** 1–9
25. Lawrence, C. W., Das, G., and Christensen, R. B. (1985) *Mol. Gen. Genet.* **200,** 80–85
26. Okada, T., Sonoda, E., Yoshimura, M., Kawano, Y., Saya, H., Kohzaki, M., and Takeda, S. (2005) *Mol. Cell. Biol.* **25,** 6103–6111
27. Hishiki, A., Hashimoto, H., Hanafusa, T., Kamei, K., Ohashi, E., Shimizu, T., Ohmori, H., and Sato, M. (2009) *J. Biol. Chem.* **284,** 10552–10560
28. Hara, K., Shimizu, T., Unzai, S., Akashi, S., Sato, M., and Hashimoto, H. (2009) *Acta Crystallogr. Sect. F* **65,** 1302–1305
29. Otwinowski, Z., and Minor, W. (1997) *Methods Enzymol.* **276,** 307–326
30. Terwilliger, T. C., and Berendzen, J. (1999) *Acta Crystallogr. D Biol. Crystallogr.* **55,** 849–861
31. Terwilliger, T. C. (2000) *Acta Crystallogr. D Biol. Crystallogr.* **56,** 965–972
32. Jones, T. A., Zou, J. Y., Cowan, S. W., and Kjeldgaard, M. (1991) *Acta Crystallogr. Sect. A* **47,** 110–119
33. Emsley, P., and Cowtan, K. (2004) *Acta Crystallogr. D Biol. Crystallogr.* **60,** 2126–2132
34. Brunger, A. T., Adams, P. D., Clore, G. M., DeLano, W. L., Gros, P., Grosse-Kunstleve, R. W., Jiang, J. S., Kuszewski, J., Nilges, M., Pannu, N. S., Read, R. J., Rice, L. M., Simonson, T., and Warren, G. L. (1998) *Acta Crystallogr. D Biol. Crystallogr.* **54,** 905–921
35. Murshudov, G. N., Vagin, A. A., and Dodson, E. J. (1997) *Acta Crystallogr. D Biol. Crystallogr.* **53,** 240–255
36. Vagin, A., and Teplyakov, A. (1997) *J. Appl. Crystallogr.* **30,** 1022–1025
37. Kraulis, P. (1991) *J. Appl. Crystallogr.* **24,** 946–950
38. Merritt, E. A., and Murphy, M. E. (1994) *Acta Crystallogr. D Biol. Crystallogr.* **50,** 869–873
39. Bond, C. S. (2003) *Bioinformatics* **19,** 311–312
40. Hardwick, K. G., and Murray, A. W. (1995) *J. Cell Biol.* **131,** 709–720
41. Chen, R. H., Shevchenko, A., Mann, M., and Murray, A. W. (1998) *J. Cell Biol.* **143,** 283–295
42. Jin, D. Y., Spencer, F., and Jeang, K. T. (1998) *Cell* **93,** 81–91
43. Luo, X., Tang, Z., Rizo, J., and Yu, H. (2002) *Mol. Cell* **9,** 59–71
44. Sironi, L., Mapelli, M., Knapp, S., De Antoni, A., Jeang, K. T., and Musacchio, A. (2002) *EMBO J.* **21,** 2496–2506
45. Luo, X., Tang, Z., Xia, G., Wassmann, K., Matsumoto, T., Rizo, J., and Yu, H. (2004) *Nat. Struct. Mol. Biol.* **11,** 338–345
46. Murakumo, Y. (2002) *Mutat. Res.* **510,** 37–44
47. Mapelli, M., Massimiliano, L., Santaguida, S., and Musacchio, A. (2007) *Cell* **131,** 730–743
48. Yang, M., Li, B., Tomchick, D. R., Machius, M., Rizo, J., Yu, H., and Luo, X. (2007) *Cell* **131,** 744–755
49. Sonoda, E., Okada, T., Zhao, G. Y., Tateishi, S., Araki, K., Yamaizumi, M., Yagi, T., Verkaik, N. S., van Gent, D. C., Takata, M., and Takeda, S. (2003) *EMBO J.* **22,** 3188–3197
50. Nelson, J. R., Lawrence, C. W., and Hinkle, D. C. (1996) *Nature* **382,** 729–731
51. Lin, W., Xin, H., Zhang, Y., Wu, X., Yuan, F., and Wang, Z. (1999) *Nucleic Acids Res.* **27,** 4468–4475
52. Acharya, N., Haracska, L., Johnson, R. E., Unk, I., Prakash, S., and Prakash, L. (2005) *Mol. Cell. Biol.* **25,** 9734–9740
53. D'Souza, S., and Walker, G. C. (2006) *Mol. Cell. Biol.* **26,** 8173–8182
54. D'Souza, S., Waters, L. S., and Walker, G. C. (2008) *DNA Repair* **7,** 1455–1470
55. Acharya, N., Haracska, L., Prakash, S., and Prakash, L. (2007) *Mol. Cell. Biol.* **27,** 8401–8408